THE JOURNAL OF BIOLOGICAL CHEMISTRY
Vol. 280, No. 2, Issue of June 3, pp. 21144–21154, 2005
Printed in U.S.A.

Crystal Structure of the Hydroxyquinol 1,2-Dioxygenase from *Nocardioides simplex* 3E, a Key Enzyme Involved in Polychlorinated Aromatics Biodegradation*

Received for publication, January 19, 2005, and in revised form, March 10, 2005
Published, JBC Papers in Press, March 16, 2005, DOI 10.1074/jbc.M500666200

Marta Ferraroni‡, Jana Seifert§, Vasili M. Travkin¶, Monika Thiel§, Stefan Kaschabek§, Andrea Scozzafava‡, Ludmila Golovleva¶, Michael Schlömann§, and Fabrizio Briganti‡‖

From the ‡Dipartimento di Chimica, Università di Firenze, Via della Lastruccia 3, Sesto Fiorentino I-50019, Italy, the §TU Bergakademie Freiberg Interdisziplinäres Ökologisches Zentrum, Freiberg D-09599, Germany, and the ¶Skryabin Institute of Biochemistry and Physiology of Microorganisms, Russian Academy of Sciences, Pushchino Moscow Region 142290, Russia

Hydroxyquinol 1,2-dioxygenase (1,2-HQD) catalyzes the ring cleavage of hydroxyquinol (1,2,4-trihydroxybenzene), a central intermediate in the degradation of aromatic compounds including a variety of particularly recalcitrant polychloro- and nitroaromatic pollutants. We report here the primary sequence determination and the analysis of the crystal structure of the 1,2-HQD from *Nocardioides simplex* 3E solved at 1.75 Å resolution using the multiple wavelength anomalous dispersion of the two catalytic irons (1 Fe/293 amino acids). The catalytic Fe(III) coordination polyhedron composed by the side chains of Tyr^{164}, Tyr^{197}, His^{221}, and His^{223} resembles that of the other known intradiol-cleaving dioxygenases, but several of the tertiary structure features are notably different. One of the most distinctive characteristics of the present structure is the extensive openings and consequent exposure to solvent of the upper part of the catalytic cavity arranged to favor the binding of hydroxyquinols but not catechols. A co-crystallized benzoate-like molecule is also found bound to the metal center forming a distinctive hydrogen bond network as observed previously also in 4-chlorocatechol 1,2-dioxygenase from *Rhodococcus opacus* 1CP. This is the first structure of an intradiol dioxygenase specialized in hydroxyquinol ring cleavage to be investigated in detail.

Hydroxyquinol (1,2,4-trihydroxybenzene) (HQ)[1] is one of the central intermediates in the degradation of a large variety of aromatic compounds. It has been detected in the breakdown of 4-hydroxybenzoate, resorcinol, salicylate, vanillate, benzoate, protocatechuate, and gentisate, by fungi such as *Trichosporon cutaneum* or *Phanerochaete chrysosporium* (1–3). In bacteria HQ has been identified as an intermediate in the degradation of mononuclear hydroxyaromatic compounds such as resorcinol and 2,4-dihydroxybenzoate (4, 5) or amino-hydroxyaromatic compounds such as 4-aminophenol (6) as well as in the degradation of hydroxylated biaryl ethers such as 2-hydroxydibenzo-*p*-dioxin and 3-hydroxydibenzofuran (7). HQ also occurs in the catabolic pathways of aromatic compounds carrying nitro groups such as in 3- and 4-nitrophenol or as 4-nitrocatechol (8–12).

HQ and its chloro-substituted derivatives 5-chlorohydroxyquinol (5CHQ) and 6-chlorohydroxyquinol (6CHQ) play an especially important role in the bacterial degradation of phenols or phenoxyacetates carrying a chloro-substituent in *para* position to the OH or OCH_2COO^- group, respectively. Thus, pentachlorophenol by rhodococci and mycobacteria has been reported to be degraded via HQ (13–16), whereas in *Sphingobium chlorophenolicum* (*Sphingomonas chlorophenolica*) already the 2,6-dichloroquinol appears to be subject to ring cleavage and, in contrast to earlier reports, no 6CHQ is formed (17). On the contrary, for 2,4,6-trichlorophenol breakdown 6CHQ has been suggested as an intermediate for *Streptomyces rochei* 303 as well as several Gram-negative bacteria (18–24). 2,6-Dichlorophenol can also be degraded via 6CHQ, whereas 2,4-dichlorophenol, 4- and 2-chlorophenol by 2,4,6-trichlorophenol-induced cells may be transformed on the same pathway, but yielding HQ as a ring cleavage substrate (18, 19, 24). In 2,4,5-trichlorophenoxyacetate degradation by *Burkholderia* (*Pseudomonas*) *cepacia* AC1100 5CHQ and HQ are formed sequentially as intermediates (25). Although 3,5-dichlorohydroxyquinol was found to be an intermediate of 2,4-dichlorophenoxyacetate degradation by *Nocardioides simplex* 3E, HQ may also be involved as a ring cleavage substrate (26, 27).

HQs are degraded aerobically by specialized intradiol ring-cleaving dioxygenases; the most studied enzymes from this family are the protocatechuate 3,4-dioxygenases (3.4-PCDs), the catechol 1,2-dioxygenases (1,2-CTDs), and the chlorocatechol 1,2-dioxygenases (1,2-CCDs) which generally possess distinctive substrate specificities (28). The hydroxyquinol 1,2-dioxygenases (1,2-HQDs hereafter) catalyze the intradiol cleavage of hydroxyquinols to form 3-hydroxy-*cis,cis*-muconates, which occur in solution in the keto form, *i.e.* as maleylacetate (Scheme 1) (29).

Several 1,2-HQDs have been purified and characterized from

* This work was supported by Grant ICA2-CT-2000-10006 from the European Commission Research and Technological Development Program Copernicus, Contract HPRI-CT-1999-00017 from the European Community Access to Research Infrastructure Action of the Improving Human Potential Program to the EMBL Hamburg outstation, and Grant COFIN2002 from the Italian Ministero Università e Ricerca Scientifica. The costs of publication of this article were defrayed in part by the payment of page charges. This article must therefore be hereby marked "*advertisement*" in accordance with 18 U.S.C. Section 1734 solely to indicate this fact.

The atomic coordinates and structure factors (code 1TMX) have been deposited in the Protein Data Bank, Research Collaboratory for Structural Bioinformatics, Rutgers University, New Brunswick, NJ (http://www.rcsb.org/).

‖ To whom correspondence should be addressed. Fax: 39-055-457-3333; E-mail: fabrizio.briganti@unifi.it.

[1] The abbreviations used are: HQ, hydroxyquinol; 1,2-CCD, chlorocatechol 1,2-dioxygenase; 5CHQ, 5-chlorohydroxyquinol; 6CHQ, 6-chlorohydroxyquinol; 1,2-CHQD, chlorohydroxyquinol 1,2-dioxygenase; 1,2-CTD, catechol 1,2-dioxygenase; 1,2-HQD, hydroxyquinol 1,2-dioxygenase; MAD, multiple wavelength anomalous dispersion; 3,4-PCD, protocatechuate 3,4-dioxygenase.

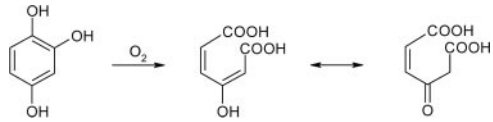

SCHEME 1

a variety of microorganisms such as Gram-negative bacteria (*B. cepacia* AC1100, *Azotobacter sp*. GP1, *Ralstonia pickettii* DTP0602, *Burkholderia* sp. strain AK-5), Gram-positive bacteria (*S. rochei* 303, *N. simplex* 3E, *Arthrobacter* sp. strain BA-5-17) and also from fungi (*T. cutaneum*, *P. chrysosporium*), but very little is known about the factors controlling substrate specificity for this novel group of intradiol dioxygenases (1, 2, 6, 20, 24, 25, 30–32). 1,2-HQD from *N. simplex* 3E is a homodimer with a molecular weight of about 65,000, containing Fe(III) ions essential for its activity with quaternary structure (α Fe(III))$_2$ (30). X-ray absorption spectroscopy studies showed that in the native enzyme as well as in the enzyme-substrate complex, the iron is pentacoordinated, with an average Fe-L distance of 1.93 Å and that histidines are present in the metal coordination sphere (2, 33).

To date, structural information is available only for a few intradiol dioxygenases from the 3,4-PCD and the 1,2-CTD families. The 3,4-PCD family has been studied extensively with enzymes from *Pseudomonas aeruginosa,* and *Acinetobacter* "*calcoaceticus*" ADP1*;* their adducts with substrates and inhibitors were also characterized (34–40). For the 1,2-CTD family the structures of catechol 1,2-dioxygenase from *Acinetobacter calcoaceticus* ADP1 (*Ac* 1,2-CTD hereafter) and 4-chlorocatechol 1,2-dioxygenase from *Rhodococcus opacus* 1CP (*Rho* 1,2-CCD) have been solved recently (41, 42).

DNA sequencing showed that 1,2-HQDs are most closely related to catechol and chlorocatechol dioxygenases (7, 11, 21, 31, 32, 43). Nevertheless, 1,2-HQDs appear to have a distinct substrate specificity and do not, or relatively slowly, convert catechol or substituted catechols, respectively (1, 2, 6, 7, 20, 22, 24, 25, 30–32). Because 1,2-HQDs on one hand and (chloro)-catechol dioxygenases on the other belong to different catabolic pathways, and correspondingly, the respective genes belong to different operons, the development of HQD substrate specificity was a very important step in the evolution of pathways for the efficient biodegradation of natural aromatic compounds as well as of xenobiotics. The analysis of the first crystal structure of a 1,2-HQD from *N. simplex* 3E (hereafter *Ns* 1,2-HQD), an enzyme that catalyzes the degradation of HQ with markedly high selectivity (30), could shed some light on the structural factors governing substrate specificity in a group of enzymes that catalyze key reactions in the biodegradation of toxic compounds.

EXPERIMENTAL PROCEDURES

Strain, Protein Preparation, and Sequencing of N Terminus and Peptides—Growth of the 2,4,5-trichlorophenoxyacetic acid utilizing strain *N. simplex* 3E with 2,4-dichlorophenoxyacetic acid as an alternative carbon source has been reported previously (44). 1,2-HQD from *N. simplex* 3E was purified as reported previously (30). Tryptic peptides were isolated as described for other enzymes (45, 46) using 1 mg of 1,2-HQD for the digestion. Sequencing of the N terminus and of tryptic peptides was performed using an Applied Biosystems model 473A sequencer.

Cloning and Sequencing of the 1,2-HQD Gene—General methods for isolation and manipulation of DNA and cultivation of *Escherichia coli* cells were as reported previously (47). pBluescript II SK(+) obtained from Stratagene was used as general cloning vector, and a T vector (48) derived from it was used for cloning PCR products. Recombinant plasmids were transformed into *E. coli* DH5α, bought from Invitrogen. Genomic DNA from *N. simplex* 3E was prepared by the method of Wilson (49).

Primers for the amplification of the 1,2-HQD gene were designed for conserved regions of the 1,2-HQDs of *R. pickettii* (*hadC*), *Arthrobacter* sp. strain BA-5-17, *Sphingomonas wittichii* RW1 (*dxnF*), *B. cepacia* (*tftH*), and *Agrobacterium tumefaciens* C58 (7, 31, 32, 43). Primer HQD-fw1 (5′-CGS CAG GAR TKS ATC CTG-3′) targets the bases corresponding to amino acid positions 82–87 in the alignment (see Fig. 4), whereas primer HQD-rev1 (5′-CCR TCR KNM GGN ATS GGR TA-3′) is expected to bind to the bases corresponding to positions 219–224 in the alignment (see Fig. 4). Thus, the PCR products had an expected length of about 400 bp.

The PCR mixture (50 μl) contained 30 pmol of each primer, 0.5 μg of genomic template DNA, 20 μM each deoxynucleotide triphosphate, 1 × PCR buffer (MBI Fermentas), 1.0 unit of DNA Taq polymerase (MBI Fermentas), 1.5 mM $MgCl_2$, 5% dimethyl sulfoxide, and 0.5% bovine serum albumin. The PCR was performed with a touchdown thermocycle program: an initial denaturation (95 °C, 5 min); 10 cycles with decreasing annealing temperature (60–50 °C, 30 s), polymerization (72 °C, 1 min), and denaturation (95 °C, 30 s); 20 more cycles with 50 °C as the annealing temperature; and an additional 5 min of polymerization during the last cycle.

After cloning of the 400-bp PCR product into a T vector, giving rise to plasmid pNocSi01, sequencing of the fragment proved it to be homologous to the corresponding segments of other 1,2-HQD genes. Labeling of the 400-bp fragment by a DIG DNA Labeling and Detection Kit Nonradioactive (Roche Applied Science) was performed as described in the Roche manual. The probe was then used to detect the corresponding fragment on a Southern blot of 0.64 μg of *N. simplex* 3E DNA digested with BamHI, PstI, SacI, and XhoI, respectively, and run on a 1% agarose gel with 1*TAE buffer (47). From a second gel, an area that corresponded in size to the hybridization signal (3 kb, SacI) was excised, and the included DNA was eluted and ligated into the dephosphorylated SacI site of pBluescript II SK(+). After transformation of the ligation mixture into *E. coli* DH5α, the labeled insert of pNocSi01 was used to identify clone pNocSi89 by colony hybridization.

The nucleotide sequence of the 1,2-HQD was determined by preparing subclones of pNocSi89 with the restriction enzymes SacII and XhoI. Two different 650-bp SacII restriction fragments and a 1.2-kb XhoI fragment, respectively, encode the complete sequence of the gene. For sequencing reactions, a MBI Fermentas CycleReader Auto DNA Sequencing Kit was used, with subsequent electrophoresis with a Li-cor 4200 IR^2 sequencer and analysis with the e-Seq program (version 1.2). Sequences were assembled using Staden Package version 2002.0. The sequence is available under GenBank/EMBL/DDBJ accession number AY822041. Comparisons with data-base entries were performed by using BLASTX (50). Multiple sequence alignments were created using ClustalX (version 1.8) (51).

Crystallization and Data Collection—The enzyme was crystallized at 293 K using the sitting drop vapor diffusion method from a solution containing 2.0 M ammonium sulfate, 4% polyethylene glycol 400, 100 mM Hepes pH 7.5 (52). The drops consisted of 4 μl of 20 mg/ml protein solution and 6 μl of reservoir solution equilibrated against 50 μl of reservoir solution (Crystal Clear Strips from Molecular Dimension, Inc.).

A native data set extending to a maximum resolution of 1.75 Å was collected at the X11 beamline, EMBL, DESY, Hamburg. Data were collected using a MAR CCD165 detector at a wavelength of 0.908 Å. Crystals belong to the primitive monoclinic space group $P2_1$ with unit cell dimensions a = 46.28, b = 84.98, c = 83.92 Å, β = 92.84°. For all data collections crystals of the native enzyme were cooled at 100 K adding 17% ethylene glycol to the mother liquor solution as cryoprotectant. Crystals suffered from damage if they were transferred in solution different from their mother solution unless they were previously cross-linked adding glutaraldehyde to the drops up to a final concentration of roughly 2% (v/v).

Metal Content Analysis—Analysis of the protein metal content was performed by using a PerkinElmer Optima 2000 Inductively Coupled Plasma AES (Atomic Emission Spectrometry) Dual Vision. The metal content analysis revealed the presence of 2 equivalents of iron ions and 1 equivalent of copper ions/mol of protein.

Structure Determination and Refinement—All molecular replacements attempts, using coordinates of known intradiol dioxygenases structures as a model, failed to provide a solution for *Ns* 1,2-HQD.

The structure of the enzyme was, therefore, solved by multiple wavelength anomalous dispersion (MAD) using the anomalous signal of the two catalytic irons. MAD data were collected at the BM14 beamline, ESFR, Grenoble. The data collected at three wavelengths (inflection, peak, remote) were processed and integrated with DENZO and scaled by SCALEPACK, from the HKL program suite (53).

The program SOLVE (54) was used to identify the two iron sites and

TABLE I
Summary of data collection and atomic model refinement statistics

Data collection	Native	Fe peak	Fe inflection	Fe remote
Wavelength (Å)	0.908	1.738	1.741	1.001
Limiting resolution (Å)	1.75	2.6	2.6	2.2
Unique reflections	61,454	18,841	18,768	35,271
R_{sym}(%)	4.6 (11.0)[b]	6.4 (21.4)	6.2 (19.1)	4.7 (31.0)
Multiplicity	4.3	5.1	3.2	3.7
Completeness overall (%)	94.1 (69.6)	99.5 (95.7)	99.1 (91.8)	99.8 (98.3)
$\langle I/\sigma(I)\rangle$	22.2 (6.4)	18.4 (4.2)	14.4 (3.4)	23.3 (3.6)
Overall figure of merit				
Before density modification		0.56		
After density modification		0.82		
Refinement				
Resolution range (Å)		20.0–1.75		
Unique reflections, working/free		56,787/2,988		
R factor (%)		19.2		
R_{free} (%)		24.6		
No. of non-hydrogen atoms		4,541		
No. of water molecules		837		
r.m.s.d.[a] bond length (Å)		0.017		
r.m.s.d. bond angle (°)		1.588		

[a] r.m.s.d., root mean square difference.
[b] Numbers in parentheses are for the highest resolution shell.

for phase calculation. The 2.6 Å MAD phases were improved and extended to 2.2 Å by solvent flattening and histogram mapping using the program DM from the CCP4 program suite (55). Automatic tracing was performed initially with the program RESOLVE (56) and extended using ARP/WARP version 6.0 (57). After 200 cycles of refinement and 20 cycles of autobuilding, 532 amino acids of 586 were found and placed in 16 chains with a global connectivity index of 0.94. After this process manual intervention was required to complete the model. The model was initially refined against 2.2 Å resolution (MAD remote wavelength data set) and finally against 1.75 Å data, using the program Refmac 5.1.24 from the CCP4 program suite (55). Manual rebuilding of the model was performed using the program QUANTA (58). Solvent molecules were introduced automatically using ARP (57). Refinement resulted in R factor and R_{free} values of 19.2 and 24.6%, respectively. Data processing and refinement statistics are summarized in Table I. The overall mean B factor of the structure after refinement was 25.68 Å^2 for chain A, 28.23 Å^2 for chain B, and 29.15 Å^2 for all atoms.

Protein coordinates have been deposited in the Protein Data Bank (accession number 1TMX).

The final model is composed of residues 2–293 for chain A and 4–293 for chain B, two Fe(III) ions, two benzoate ions, two phospholipids (C13/C17), two sulfate ions, one copper ion, one chloride ion, and 837 water molecules.

There are two disordered regions in chain B corresponding to residues 67–72 and 263–275. Electron density was missed for residues B264, B265, and B270 even for the main chain atoms, and they were not introduced in the model. Furthermore, no electron density was visible for the side chains of residues: A2 Ser, A73 Glu, B8 Glu, B71 Thr, B72 Asn, B75 Arg, B95 Asn, B264 Arg, B266 Pro, B276 Gln, and B277 Ile.

Double conformations for the side chains of residues A118 Arg, A155 Val, A195 Lys, A222 Leu, A244 Glu, A247 Asp, A285 Arg were modeled.

A spheric electron density in the $F_o - F_c$ map at 12σ was found bound to His A42 (2.12 Å) and His B42 (2.02 Å), and it could be easily attributed to a metal ion. A peak at lower height, compared with the iron ones, was present in the Harker section of the anomalous Patterson maps corresponding to the position of the metal ion. The metal should be one close to the iron as number of electrons because of the height of the peak in the $F_o - F_c$ map (assuming a unitary occupancy) and because it should have an absorption edge near to the iron K edge. The coordination sphere of the metal is completed by a chloride ion (2.57 Å).

An electron density was found close to the iron in both active sites, and it was explained as a benzoate-like molecule bound to the iron in a bidentate way.

Two sulfate ions were found on the surface of the A chain, hydrogen bonded to some water molecules and side chain atoms.

Structure Analysis—The stereochemical quality of the models was assessed using the program PROCHECK (59). The Ramachandran plot is of a good quality, with 479 non-glycine and non-proline residues; among these, 438 (91.4%) are in the most favored regions, 38 (7.9%) are in the additional allowed regions, 1 (2%) (Thr B71) is in the generously allowed regions, and 2 (4%) (Glu B73 and Arg B74) are in disallowed regions.

The secondary structure was defined utilizing the DSSP data base and program (60).

Global structure superimpositions were carried out by utilizing the matching algorithm implemented into the HEX 4.2 program (61). Least squares fits of the active site regions were performed using the McLachlan algorithm as implemented in the program ProFit 2.2 (www.bioinf.org.uk/software/profit/) specifying as the fitting subset the four amino acid ligands to the catalytic iron ions (62).

Electrostatic Potentials were estimated first transforming the protein data base coordinate file into a pqr file containing partial charges and radii for each atom by using the PDB2PQR web service and then solving the second order differential Poisson-Boltzmann equation, which relates the electrostatic potential in a dielectric to the charge density using the macroscopic electrostatics with atomic details (MEAD) program package (63, 64).

HQ was docked manually into the active site by first simulating the dissociation of Tyr^{197} from the iron center. It was assumed that the substrates bind to the iron in a bidentate fashion and with orientations of their aromatic ring similar to those observed for catechol or 4-methylcatechol in *Ac* 1,2-CTD or for the benzoate ion in *Ns* 1,2-HQD and *Rho* 1,2-CCD (41, 42). Slight rotations and/or tilts of the iron-bound substrate molecules did not result in changes in the amino acid residues interacting with the substrates ring substituents.

PyMol, UCSF Chimera, and MS/MS were used to produce ribbon diagrams, electrostatic potential surfaces, electron density and other representations (65–67).

RESULTS AND DISCUSSION

Gene and Protein Sequence—Using primers directed toward regions conserved in other 1,2-HQDs, it was possible to amplify a segment of the expected size (400-bp) from genomic DNA of *N. simplex* 3E. The use of this fragment as a probe allowed us to clone a 3-kbp fragment of *N. simplex* 3E DNA into *E. coli*. Sequencing of two 650-bp and a 1.2-kbp region from several subclones resulted in the complete sequence of the presumed 1,2-HQD gene.

Independently from the genetic approach, the following sequences were obtained by amino acid sequencing of the N terminus and of nine tryptic peptides of the purified protein (amino acids separated by slashes or *X* indicating uncertain positions): 1,2-HQD-27 (S/*X* A A/D S/*X* LN S/*X*), 1,2-HQD-36 (SFDATADPR *X*/R), 1,2-HQD-51 (A/E I T/D P/G TP), 1,2-HQD-55 (IESGGDI), 1,2-HQD-61/63 (IEV W/*X* EADDDGFY D/*X* VQYDD D/*X*), 1,2-HQD-70 (A/L T/H E/L A/L E/S), 1,2-HQD-72 (TLVT*X*IF M/F), 1,2-HQD-77 (RQEFILL). All of these peptides, except 1,2-HQD-27 (for which the sequence was of low quality), occur in the sequence predicted from the cloned *N. simplex* 3E gene (as well as in those from the *tftH*, *hadC*, *dxnF* genes), thus proving that, in fact, the gene of a 1,2-HQD was cloned and sequenced.

The most similar sequence in the data base was that of

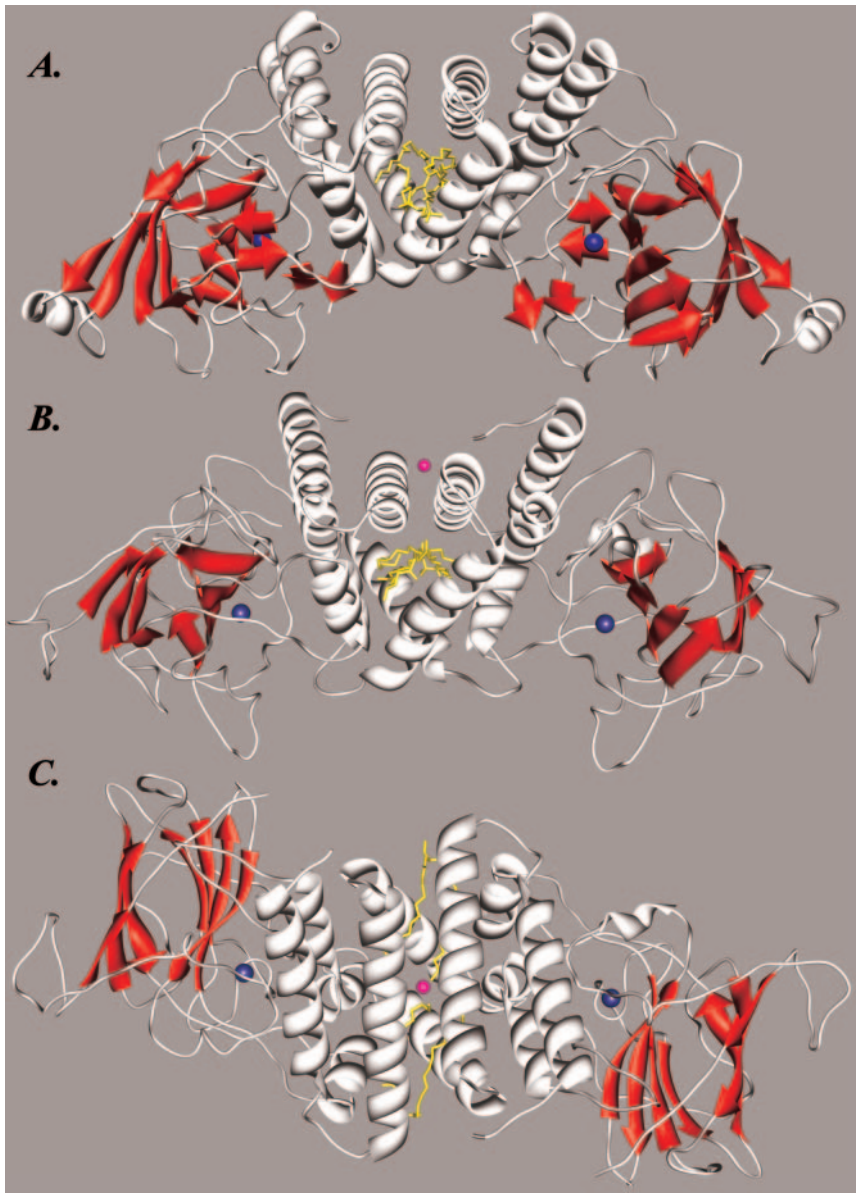

FIG. 1. **Schematic representation of the overall structure of *Ac* 1,2-CTD (*A*), *Ns* 1,2-HQD (*B*), 90° rotated *B* around the horizontal axis (*C*).** The iron and copper ions are represented as *blue* and *magenta spheres*, respectively; the phospholipid molecules are shown in *yellow*.

1,2-HQD from *Arthrobacter* sp. strain BA-5-17 (32) (73% identical positions in the alignment of Fig. 4). The similarity to other 1,2-HQDs ranged from 42 to 69% identical positions (see alignment of Fig. 4). In contrast, the similarity to the representatives of catechol and chlorocatechol 1,2-dioxygenases given in Fig. 4 was between 22 and 30% identical positions.

Overall Structure and Linker Domain—The 1,2-HQD from the Gram-positive bacterium *N. simplex* 3E is a homodimeric protein with overall dimensions 110 × 50 × 50 Å. The statistics for data collection, phasing, and structure refinement are summarized in Table I. The final model is composed of residues 2–293 for chain A and 4–293 for chain B, two Fe(III) ions, one copper ion, two benzoate ions, two phospholipids (C13/C17), two sulfate ions, one chloride ion and 837 water molecules.

The general topology of *Ns* 1,2-HQD resembles that of *Ac* 1,2-CTD and comprises two catalytic domains separated by a common "α-helical zipper" motif that consists of six N-terminal helices from each subunit.

Two phospholipid molecules are located inside a large hydrophobic channel formed by the two protein monomers at the interface between the two subunits and in the center of the linker domain, with the head group directed outward into the solvent and the tail moieties pointing inward, toward each other (Fig. 1). A phosphatidylcholine molecule with two C12–13/C17 hydrophobic tails was used as a model because the absence of the electron density of the head groups did not allow determination of their precise identity, and the length of each tail was based on the length of the electron density and on the stereochemistry of known phospholipids. The presence of such phospholipids appears to be distinctive for this class of enzymes, although their possible role has still to be clarified (41, 42).

The linker domain is mainly composed of three long (H1–H3) and three short (H4–H6) α-helices supplied by each subunit: five helices from the N terminus of each monomer are interacting with the equivalent motif from the other subunit and with the sixth helix, which elongates from the catalytic domain (Figs. 1 and 2). A metal ion bound to both His^{42} (at 2.01 and 2.12 Å) from helices H2 of both subunits and to a chloride ion (at 2.57 Å) is shown in Fig. 1. The protein metal content analysis (see "Experimental Procedures") and the trigonal coordination geometry observed suggest that such metal ion is copper in an oxidation state I. Its location suggests a possible structural role in stabilization of the enzyme quaternary assembly for such metal ion.

Fig. 2 shows the three-dimensional structural least squares

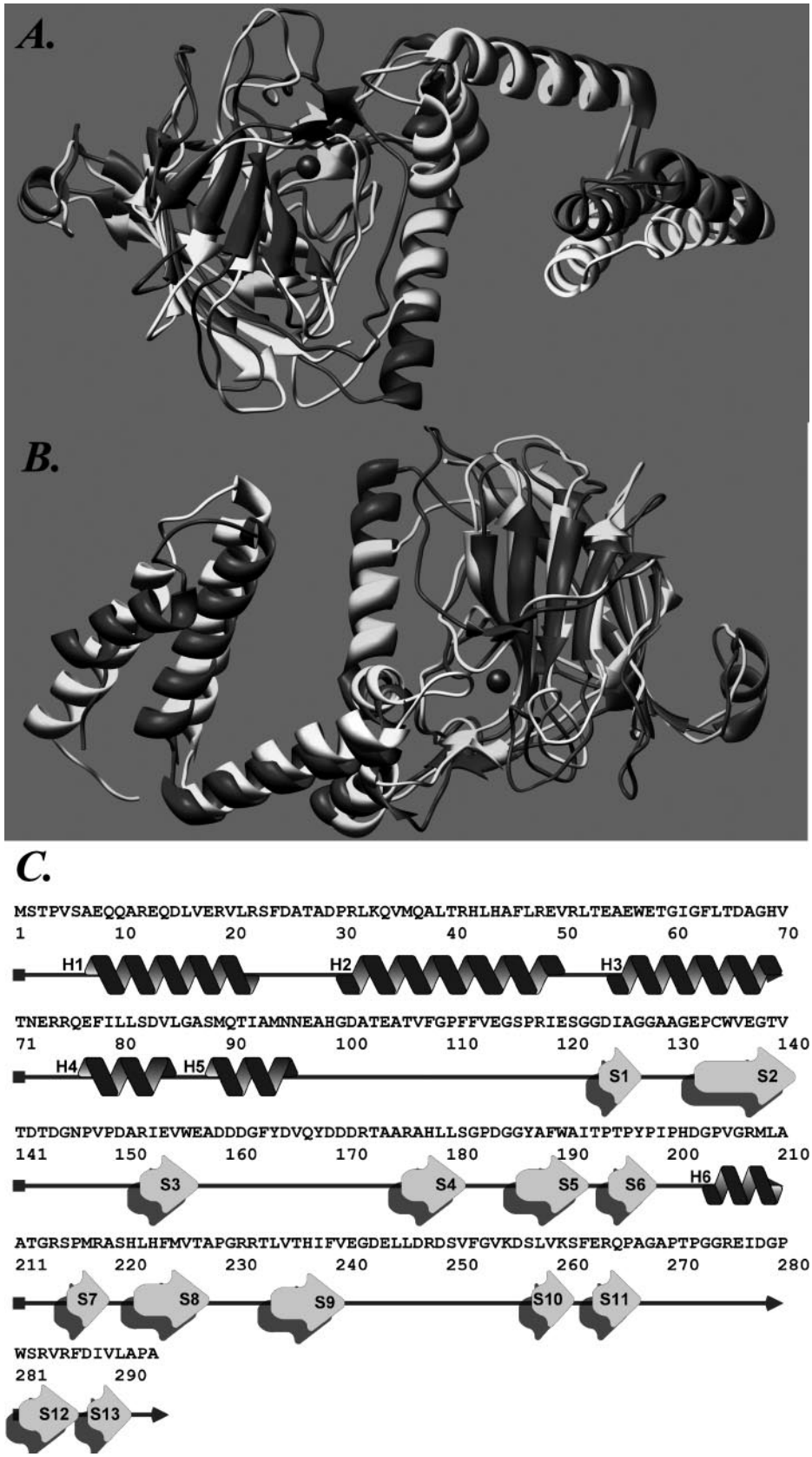

FIG. 2. Least squares superimposition of a single subunit of *Ac* 1,2-CTD (*dark*) and *Ns* 1,2-HQD (*light*) in two different orientations (*A* and *B*). *C*, schematic representation of the secondary structure of *Ns* 1,2-HQD as assigned by the program DSSP (60).

superposition of a single subunit of *Ns* 1,2-HQD and *Ac* 1,2-CTD. The first N-terminal α-helix H1 and the random coil region preceding the α-helix H4 extending from the central domain are longer in *Ns* 1,2-HQD compared with *Ac* 1,2-CTD. About one-half of the fifth helix (H5) is missing compared with the corresponding one from *Ac* 1,2-CTD. The first two short β-sheets in *Ac* 1,2-CTD are also missing in *Ns* 1,2-HQD, being substituted by random coil regions. The secondary structure of the central section of *Ns* 1,2-HQD thoroughly resembles that of the 1,2-CTD family. Finally, the C-terminal region of *Ns* 1,2-HQD, as observed also in the *Rho* 1,2-CCD, the only representative of chlorocatechol cleaving dioxygenases for which the three-dimensional structure is

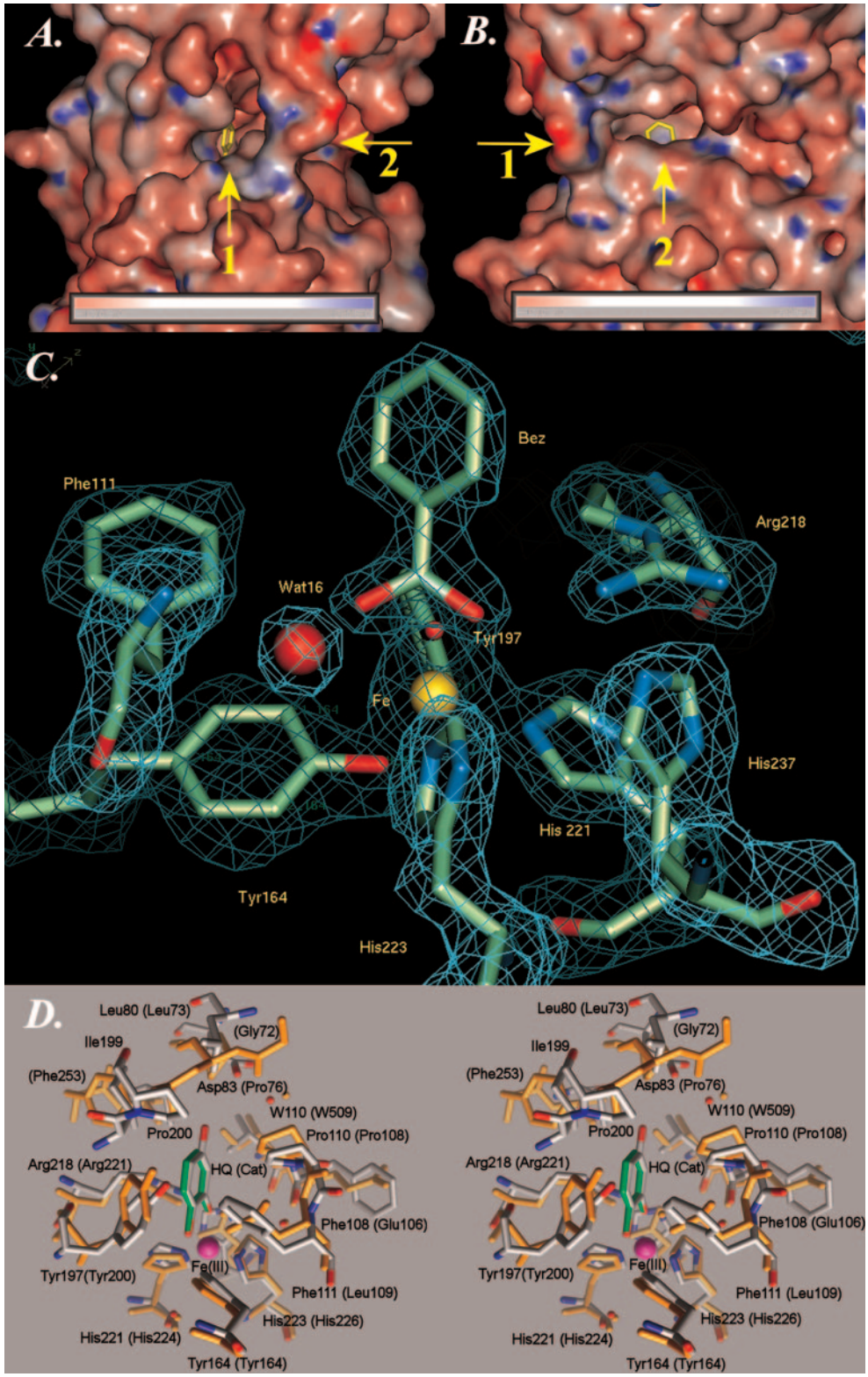

FIG. 3. *A* and *B*, representations of the two active site entrances of *Ns* 1,2-HQD. The surface is color-coded on the basis of the calculated electrostatic potential. The *blue* color corresponds to positive and *red* to negative potentials. The benzoate-like molecule is depicted in *yellow*. *A* and *B* show 90° vertically rotated views of the enzyme, and the two active site entrances are indicated by *yellow arrows*. *C*, $F_o - F_c$ electron density map for the active site of *Ns* 1,2-HQD. The electron density is contoured at the 3σ level. *D*, stereo representation of the superposed active sites structures of HQ docked to *Ns* 1,2-HQD and of the catechol complex of *Ac* 1,2-CTD (*orange* colored, PDB code 1DLT). Designations of amino acids positions are first given for *Ns* 1,2-HQD and second (in parentheses) for *Ac* 1,2-CTD.

known, lacks the seventh helix, the last long random coil, and the final β-sheet present in *Ac* 1,2-CTD (42).

The Catalytic Domain—Each subunit contains one catalytic pocket accessible to the substrate from the hollow side of the dimer. The central part of the catalytic domain is made up of several β-sheets arranged in a β-sandwich conformation and by a number of random coils positioned between the linker domain and the β-sheets assembly (see Figs. 1 and 2). The active site

TABLE II

Bond distances and angles of the catalytic iron ion coordination polyhedron for Ns 1,2-HQD (compared with Ac 1,2-CTD)

See Ref. 41.

	Distance *X*-Fe(*Ac* 1,2-CTD)	Angle*X*-Fe-Tyr^{164}	Angle *X*-Fe-Tyr^{197}	Angle *X*-Fe-His^{221}	Angle *X*-Fe-His^{223}
	Å	*degrees*	*degrees*	*degrees*	*degrees*
Tyr^{164} (164)	1.95 (1.85)		100.63	103.4	86.13
Tyr^{197} (200)	2.01 (2.20)			95.4	171
His^{221} (224)	2.11 (2.15)				88.7
His^{223} (226)	2.24 (2.0)				
Benz O1	2.13				
Benz O2	2.59				

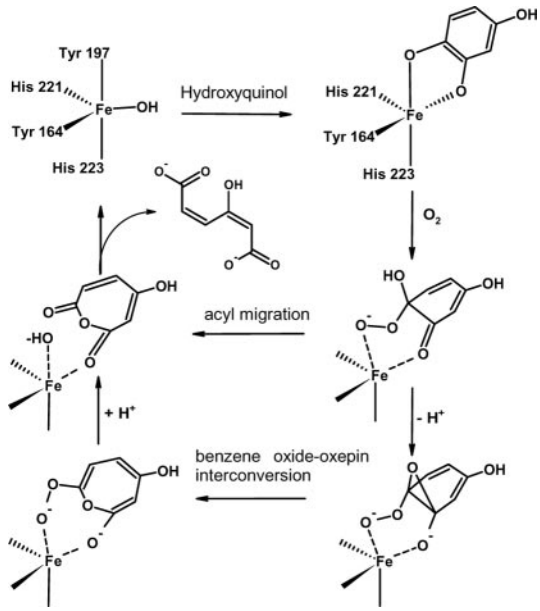

SCHEME 2

metal center is located in the random coils region flanked on one side by the β-sandwich motif of each monomer and on the other side by the α-helices of the linker domain.

Each catalytic pocket of *Ns* 1,2-HQD is bordered by Leu^{80} and Asp^{83} from helix H4; Val^{107}, Phe^{108}, Pro^{110}, and Phe^{111} from a first random coil; Trp^{156} from sheet S3; Tyr^{164}, the mobile iron ligand, from a second random coil; Tyr^{197} from sheet S6; Ile^{199} and Pro^{200} from a third random coil; Arg^{218} from sheet S7; His^{221} and His^{223} from sheet S8; His^{237} from sheet S9; and Val^{251} from a fourth random coil.

As shown in Fig. 3, *A* and *B*, a distinctive feature of the present structure is that each active site presents two openings. The first one located as the one observed previously in the *Ac* 1,2-CTD and *Rho* 1,2-CCD structures and delimited by residues Leu^{80}, Pro^{110}, Phe^{111}, Pro^{198}, Ile^{199}, Pro^{200} plus the backbones of the Tyr^{164} and Tyr^{197} iron ligands; the second placed at about 90° on the right side of the first one and bordered by residues Leu^{80}, Asp^{83}, Val^{107}, Phe^{108}, Gly^{109}, and Val^{251}. A number of water molecules are present in the openings and in the upper part of the active cavity even though a benzoate-like molecule, bound to the active site iron, occupies a large part of the cavity.

Some of the active site residues, with the corresponding $F_o - F_c$ density overlaid are depicted in Fig. 3*C*. The mononuclear Fe(III) ion shows a His_2Tyr_2 coordination (Tyr^{164}, Tyr^{197}, His^{221}, and His^{223}), typical of all intradiol ring cleaving dioxygenases (28). X-ray absorption spectroscopy data collected for the same *Ns* 1,2-HQD indicate that generally the native enzyme is pentacoordinated with two spheres of atoms: either two at 1.90 Å and three at 2.06 Å, or three at 1.92 Å and two at 2.08 Å (33). In the present crystal structure, a benzoate-like ion is coordinated to the iron ion in a bidentate asymmetric mode substituting the metal bound water molecule/hydroxide ion, observed in the native 1,2-CTDs, increasing the iron coordination number to 6 (Fig. 3*C*). An equivalent molecule has also been observed recently in the active site of *Rho* 1,2-CCD. In *Ns* 1,2-HQD the benzoate ion is stabilized by a hydrogen bond network that connects the benzoate O1 atom to Arg^{218} NH1 (hydrogen-bonded further to Asp^{249}) and the benzoate O2 atom to a well ordered W16 active site water molecule (B factor = 20.63) (hydrogen-bonded further to Phe^{108}, Pro^{110}, Phe^{111}, and Trp^{156}). As observed in *Rho* 1,2-CCD the benzoate binding does not trigger the dissociation of Tyr^{197}, although causing a conformational orientation of Arg^{218} observed when substrates bind to intradiol dioxygenases, but contrarily to what observed in all 1,2-CTDs, 1,2-CCDs and 3,4-PCDs, Arg^{218}, supposed to promote the substrate positioning and deprotonation, is not stabilized by a strong hydrogen bond to a Gln because this residue is replaced by His^{237}, which is positioned a bit further away (35, 37, 38, 40, 41).

No convincing hypotheses can be made, at the moment, on the possible reasons for the presence of a benzoate-like molecule bound to the catalytic metal ion, although exogenous ligands have been often found bound to metal sites acting as stabilizers of the active enzyme by hampering metal ion dissociation. The molecule resembles benzoate or benzamide, which actually act as very weak competitive inhibitors for these enzymes, easily displaced by catechols or HQs.[2]

In Table II the distances of the iron ligands are reported: Tyr^{164} and Tyr^{197} exhibit shorter bonds (1.95 and 2.01 Å, respectively) than His^{221} and His^{223} (2.11 and 2.24 Å, respectively), and the iron coordination sphere is completed by the benzoate-like molecule asymmetrically bound with O1 (~2.13 Å) and O2 (~2.59 Å).

Substrate Specificity—The catalytic mechanism of intradiol ring-cleaving dioxygenases has been proposed to operate via Fe(III) activation of the diol substrate first generating an Fe(II) semiquinone, which reacts directly with dioxygen to give a hydroperoxide intermediate, a Criegee rearrangement via acyl migration would finally generate the corresponding muconic anhydride (Scheme 2) (68). An alternative mechanism for migration of the electron-deficient acyl group, via a benzene-oxide-oxepin interconversion, has also been proposed (Scheme 2) (69).

Substrate selection and conversion are expected to be controlled mainly by the ring substituents effects on the electron density of the carbon atoms exposed to the molecular oxygen attack as well as by the interactions of ring substituents with the surrounding active site amino acidic residues.

Although a number of studies on inhibitors, substrates, and substrate analog adducts of 3,4-PCDs and *Ac* 1,2-CTD have revealed several important features of the mechanism of exogenous ligands binding to their active site, and the structure of

[2] M. Ferraroni, A. Scozzafava, and F. Briganti, unpublished results.

TABLE III
Comparison of the substrate specificity of HQ-cleaving enzymes and two representatives of the (chloro-)catechol-cleaving enzymes

Enzyme and organism	Relative activity[a]						Ref.
	HQ	5CHQ	6CHQ	Catechol	Pyrogallol	3-Methylcatechol	
	%	%	%	%	%	%	
1,2-HQD *Azotobacter* sp. GP1	100		33	0	0	0	(20)
1,2-HQD *B. cepacia* AC1100	100	0		0			(25)
1,2-HQD *N . simplex* 3E	100	2.4	5.0	0.6		0	(27, 30)
1,2-HQD *R. pickettii* DTP0602	100		28	0	14	7 intra 10 extra	(31)
1,2-HQD *W. eutropha* JMP134	100		12				(22)
1,2-HQD *Arthrobacter* sp. BA-5–17	100			15			(32)
1,2-HQD *S. wittichii* RW1	100			45			(7)
1,2-CHQD *S. rochei* 303	100		636	0			(24)
1,2-HQD *T. cutaneum*	100			<1	<1	0	(1)
1,2-HQD *P. chrysosporium*	100	0		20	0		(2)
1,2-CTD *P. putida* (*arvilla*) C-1[b]				100	0.6	8	(72)
1,2-CCD *R. opacus* 1CP[c]				100		208	(73)

[a] Values are given relative to the activity with HQ (for 1,2-HQDs and 1,2-CHQD) or relative to catechol for 1,2-CTD or 1,2-CCD, respectively, set as 100%. If no value was given for the respective substrate by the reference, the space is left blank.
[b] Type I representative: relative activities for 4-methylcatechol, 90%; 4-chlorocatechol, 3.6%.
[c] Type II representative: relative activities for 4-methylcatechol, 242%; for 3-chlorocatechol, 14%; 4-chlorocatechol, 95%; 3,5-dichlorocatechol, 18%.

Rho 1,2-CCD has shed some light on the substrate selectivity of chlorocatechol-cleaving enzymes, no conclusive rationalization of the observed substrate specificities for intradiol-cleaving dioxygenases has been achieved so far.

1,2-HQDs structurally belong to the group of intradiol dioxygenases comprising 1,2-CTDs. 1,2-CTDs are generally divided into two types, I and II (70). Type I dioxygenases (1,2-CTDs) are relatively specific enzymes that primarily have catechol and often also a methylcatechol as substrate. Chlorinated catechols are not used or are used only at negligible rates. Type II enzymes (better known as 1,2-CCDs) are relatively nonspecific with a wider substrate range being able to convert chlorinated catechols more rapidly than catechol and to additionally accommodate a wide range of methyl- or methoxy-substituted catechols. Regarding substrate specificity, 1,2-HQDs seem to be more closely related to type I than to the type II enzymes (Table III). Unfortunately, HQ was not tested as a potential substrate for most of the catechol and chlorocatechol 1,2-dioxygenases; a catechol 1,2-dioxygenase able to oxidize HQ at about half the rate (51%) of catechol was described only for *T. cutaneum* (71).

The *Ns* 1,2-HQD, subject of the present study, is remarkably substrate-selective. The conversions of HQ (K_m = 1.2 μM, V_{max} = 55 units/mg, k_{cat} = 29 s^{-1}, and k_{cat}/K_m = 24.2 μM^{-1} s^{-1}), 5CHQ (2.4% relative to HQ activity), and 6CHQ (5.0% relative to HQ activity) are catalyzed (30). A range of catechols and variously substituted quinols were also tested as substrates but found to only act as inhibitors for HQ turnover ($K_i \sim$ 10 mM for catechols).

Table III presents the comparison of the known substrate specificity data for 1,2-HQDs and some representatives of type I and II catechol-cleaving enzymes. The 1,2-HQDs from *B. cepacia* AC1100, *Azotobacter* sp. strain GP1, and *T. cutaneum* as well as the 1,2-CHQD from *S. rochei* 303, with respect to catechol, 3-methylcatechol, or pyrogallol conversion, show relatively high substrate specificities as the enzyme from *N. simplex*. HQ is the main substrate for the first four enzymes, whereas 6-CHQD is the best substrate for the *S. rochei* dioxygenase. 6-CHQD was also a relatively good substrate for the 1,2-HQDs of *Azotobacter* sp. GP1, *N. simplex* 3E, *Wautersia eutropha* JMP134, *R. pickettii* DTP0602, but was not tested with the fungal enzymes from *T. cutaneum* and *P. chrysosporium*. The enzyme from *P. chrysosporium* was found unable to convert 5-CHQ, but accepted catechol with 20% of the activity shown toward HQ. Also, the 1,2-HQD isolated from *R. pickettii* DTP0602 presents relatively low substrate specificity, being able to catalyze the oxidation of 3-methylcatechol and pyrogallol in addition to HQ and 6-CHQ, but it is inactive toward catechol, 3- and 4-chlorocatechol, 4-methylcatechol, protocatechuate, and 2,3-dihydroxybiphenyl (31). Furthermore, the 1,2-HQD of *S. wittichii* RW1 showed a high activity with catechol (7), and that of *Arthrobacter* sp. strain BA-5-17 was shown to catalyze both the intradiol and extradiol cleavage of catechol, although the activity toward HQ was 6.8-fold higher than that toward catechol (32).

These results evidence that substrate selectivity is a very heterogeneous issue even inside the 1,2-HQD group. It appears challenging to attempt the rationalization, at the molecular level, of the structural factors responsible for the differential substrate selectivity.

The structural alignment of the active site residues of the catecholate complex of *Ac* 1,2-CTD and the HQ docked in *Ns* 1,2-HQD is shown in Fig. 3*D*. The main interactions of *Ac* 1,2-CTD with the substrate involve the following residues (respective positions in the alignment of Fig. 4 given in parentheses): Leu^{73} (87), Pro^{76} (90), Ile^{105} (119), Pro^{108} (122), Leu^{109} (123), Arg^{221} (239), Phe^{253} (272), and Ala^{254} (273). Some of these residues and some additional ones in the cavity appear to be crucial in the correct positioning of the aromatic substrate in *Ns* 1,2-HQD (respective positions in the alignment of Fig. 4 given in parentheses): Leu^{80} (87), Asp^{83} (90), Val^{107} (119), Phe^{108} (120), Gly^{109} (121), Pro^{110} (122), Phe^{111} (123), Ile^{199} (219), Pro^{200} (220), Arg^{218} (239), and Val^{251} (273). We noticed substantial changes in some of these residues with respect to the corresponding amino acids in the representative structures of 1,2-CTDs and 1,2-CCDs and specifically: Asp^{83} (position 90 in Fig. 4, Pro^{76} in *Ac* 1,2-CTD and Ala^{53} in *Rho* 1,2-CCD), Val^{107} (position 119 in Fig. 4, Ile^{105} in *Ac* 1,2-CTD and Ile^{74} in *Rho* 1,2-CCD), Phe^{108} (position 120 in Fig. 4, Glu^{106} in *Ac* 1,2-CTD and Gln^{75} in *Rho* 1,2-CCD), Phe^{111} (position 123 in Fig. 4, Leu^{109} in *Ac* 1,2-CTD and Phe^{78} in *Rho* 1,2-CCD), His^{237} (position 258 in Fig. 4, Gln^{240} in *Ac* 1,2-CTD and Gln^{210} in *Rho* 1,2-CCD), Val^{251} (position 273 in Fig. 4, Ala^{254} in *Ac* 1,2-CTD and Cys^{224} in *Rho* 1,2-CCD).

To understand which of these residues could be mainly responsible for substrate recognition, HQ was docked into the active site of *Ns* 1,2-HQD. Two different orientations are likely: if the 4-OH substituent is oriented toward the internal part of the cavity (Fig. 3*D*) it would settle into a pocket formed by Asp^{83} and Val^{251} (positions 90 and 273, respectively, in Fig. 4), but if the substituent is oriented outward, it would essentially

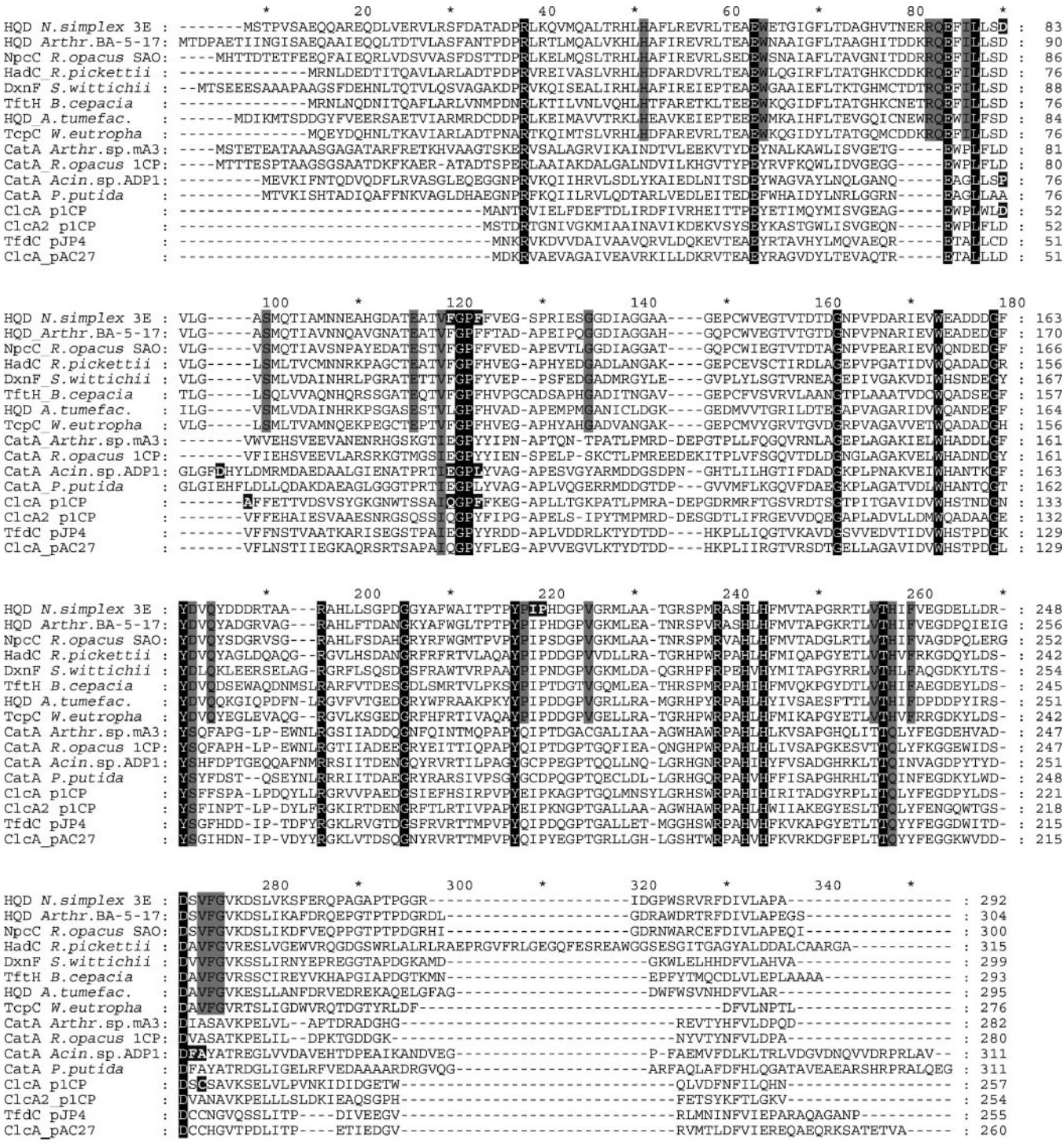

FIG. 4. **Amino acid sequence alignment of several 1,2-HQDs and representatives of catechol 1,2- and chlorocatechol 1,2-dioxygenases.** 1,2-HQD: *N. simplex* 3E (present enzyme, GenBank accession number AY822041), *Arthrobacter* sp. BA-5-17 (protein accession BAA82713), *R. opacus* SAO101 (protein accession BAD30043), *R. pickettii* DTP0602 (protein accession BAA13107), *S. wittichii* RW1 (protein accession CAA51371), *B. cepacia* AC1100 (protein accession AAC43338), *A. tumefaciens* strain C58 (protein accession AAK88258); *W. eutropha* JMP134 (protein accession AAM55216), 1,2-CTD: *Arthrobacter* sp. mA3 (protein accession JT0613), *R. opacus* 1CP (protein accession CAA67941), *Acinetobacter* sp. ADP1 (protein accession YP_046127), *Pseudomonas putida* PRS2000 (protein accession AAA66204); 1,2-CCD: *R. opacus* 1CP (p1CP) (protein accession AAC38251), *R. opacus* 1CP (p1CP) (protein accession CAD28142), *W. eutropha* JMP134 (pJP4) (protein accession AAA98262), *P. putida* AC866 (pAC27) (protein accession CAE92861). Alignment positions identical in all sequences are marked with a *black background*. Regions in which the sequences of all 1,2-HQDs are identical but differ from those of catechol or chlorocatechol 1,2-dioxygenases, or the other way around, are marked with *light gray*. Single amino acid positions marked *dark gray* are important for substrate specificity and discussed in the text.

interact with Leu[80] and Pro[110] (positions 87 and 122 in Fig. 4, Leu[73]/Leu[49] and Pro[108]/Pro[77] in *Ac* in 1,2-CTD/*Rho* 1,2-CCD, respectively). This second hypothesis seems to be unlikely because identical amino acids would interact with the substrate in the different enzymes, thus not clearly accounting for their markedly different substrate specificity. Furthermore, the orientation of HQ with the 4-OH substituent toward the internal part of the cavity is equivalent to that of bound protocatechuate in 3,4-PCDs and of bound 4-methylcatechol in *Ac* 1,2-CTD (40, 41).

A multiple sequence alignment of intradiol dioxygenases revealed several positions identical in all available 1,2-HQDs but different in one or more of the selected 1,2-CTDs or 1,2-CCDs (*shaded dark gray* in Fig. 4). Such positions may be conserved without a specific selection pressure, but they also may be of importance for the substrate specificity without a structural reason for it so far having been elucidated.

The presence of Asp^{83} and Val^{251} (positions 90 and 273 in Fig. 4), the residues expected to interact with substituents in position 4 (Pro^{76}/Ala^{53} and Ala^{254}/Cys^{224} in *Ac* 1,2-CTD/*Rho* 1,2CCD, respectively), based on structural comparisons should be mainly responsible for the selective preference for HQs. Valine residues corresponding to Val^{251} (position 273 in Fig. 4) occur in all available 1,2-HQDs, but not in the (chloro-)catechol dioxygenases, a distribution supporting the conclusions drawn from structural comparisons.

Also, 3,4-PCDs are selective for a substrate carrying a hydrophilic substituent in a distal position with respect to the diol: protocatechuate. It has been shown that the carboxyl group of protocatechuate forms a hydrogen bond with Tyr^{324} (substituted by Asp^{83} in 1,2-HQD), and its negative charge is complemented by long range electrostatic interactions with Arg^{133}, Arg^{330}, and Arg^{450} (*Ac* 3,4-PCD numbering) (40). In *Ns* 1,2-HQD Asp^{83} could have a function similar to that of Tyr^{324} in 3,4-PCDs, although in the case of HQ the substrate should not be charged at neutral pH but, Asp^{83} would.

The other feature crucial for HQ selection and limited affinity for catechols is the presence of the second large active site opening caused by the substitution and spatial reallocation of residues Gly^{72} and Asp^{81} in *Ac* 1,2-CTD with Ile^{79} and Ser^{88}, amino acids specifically conserved in all 1,2-HQDs (positions 86 and 100, respectively in Fig. 4). Contributing to the second large active site opening is a marked shift of Pro^{110} (position 122 in Fig. 4, Pro^{108} in *Ac* 1,2-CTD). The resulting larger solvent exposition of the upper part of the cavity should electrostatically favor HQ settling and stabilization.

CONCLUSIONS

The crystal structure of *Ns* 1,2-HQD evidences significant differences with respect to the known 1,2-CCD and 1,2-CTD enzymes. Several secondary structure differences are noticed, but more importantly a number of residues within the active cleft and believed to be responsible for substrate selection are altered. Leu^{80}, Asp^{83}, Val^{107}, Phe^{108}, Gly^{109}, Pro^{110}, Phe^{111}, Ile^{199}, Pro^{200}, Arg^{218}, and Val^{251} seem to be directly involved in interactions with substrates. Few amino acid differences (Asp^{83} and Val^{251}) between the *N. simplex* enzyme which exhibits a marked selectivity toward HQ, 1,2-CCDs (Ala^{53} and Cys^{224}, respectively, in *Rho* 1,2CCD) and 1,2-CTDs (Pro^{76} and Ala^{254}, respectively, in *Ac* 1,2-CTD) as well as the extensive solvent exposure of the upper part of the catalytic site are believed to be responsible for the observed substrate selectivity differences among 1,2-HQDs and the other intradiol ring-cleaving dioxygenases.

Acknowledgments—We thank V. Nödinger and R. Schmid, Universität Stuttgart, for N-terminal and peptide sequencing.

REFERENCES

1. Sze, I. S., and Dagley, S. (1984) *J. Bacteriol.* **159,** 353–359
2. Rieble, S., Joshi, D. K., and Gold, M. H. (1994) *J. Bacteriol.* **176,** 4838–4844
3. Anderson, J. J., and Dagley, S. (1980) *J. Bacteriol.* **141,** 534–543
4. Chapman, P. J., and Ribbons, D. W. (1976) *J. Bacteriol.* **125,** 975–984
5. Stolz, A., and Knackmuss, H. J. (1993) *FEMS Microbiol. Lett.* **108,** 219–224
6. Takenaka, S., Okugawa, S., Kadowaki, M., Murakami, S., and Aoki, K. (2003) *Appl. Environ. Microbiol.* **69,** 5410–5413
7. Armengaud, J., Timmis, K. N., and Wittich, R. M. (1999) *J. Bacteriol.* **181,** 3452–3461
8. Chauhan, A., Samanta, S. K., and Jain, R. K. (2000) *J. Appl. Microbiol.* **88,** 764–772
9. Chauhan, A., Chakraborti, A. K., and Jain, R. K. (2000) *Biochem. Biophys. Res. Commun.* **270,** 733–740
10. Jain, R. K., Dreisbach, J. H., and Spain, J. C. (1994) *Appl. Environ. Microbiol.* **60,** 3030–3032
11. Kitagawa, W., Kimura, N., and Kamagata, Y. (2004) *J. Bacteriol.* **186,** 4894–4902
12. Meulenberg, R., Pepi, M., and de Bont, J. A. (1996) *Biodegradation* **7,** 303–311
13. Apajalahti, J. H., and Salkinoja-Salonen, M. S. (1987) *J. Bacteriol.* **169,** 5125–5130
14. Uotila, J. S., Kitunen, V. H., Coote, T., Saastamoinen, T., Salkinoja-Salonen, M., and Apajalahti, J. H. (1995) *Biodegradation* **6,** 119–126
15. Häggblom, M. M., Janke, D., and Salkinoja-Salonen, M. (1989) *J. Bacteriol.* **55,** 516–519
16. Uotila, J. S., Kitunen, V. H., Saastamoinen, T., Coote, T., Häggblom, M. M., and Salkinoja-Salonen, M. S. (1992) *J. Bacteriol.* **174,** 5669–5675
17. Xun, L., Bohuslavek, J., and Cai, M. (1999) *Biochem. Biophys. Res. Commun.* **266,** 322–325
18. Golovleva, L. A., Zaborina, O., Pertsova, R., Baskunov, B., Schurukhin, Y., and Kuzmin, S. (1992) *Biodegradation* **2,** 201–208
19. Kiyohara, H., Hatta, T., Ogawa, Y., Kakuda, T., Yokoyama, H., and Takizawa, N. (1992) *Appl. Environ. Microbiol.* **58,** 1276–1283
20. Latus, M., Seitz, H.-J., Eberspächer, J., and Lingens, F. (1995) *Appl. Environ. Microbiol.* **61,** 2453–2460
21. Louie, T. M., Webster, C. M., and Xun, L. (2002) *J. Bacteriol.* **184,** 3492–3500
22. Padilla, L., Matus, V., Zenteno, P., and Gonzalez, B. (2000) *J. Basic Microbiol.* **40,** 243–249
23. Xun, L., and Webster, C. M. (2004) *J. Biol. Chem.* **279,** 6696–6700
24. Zaborina, O., Latus, M., Eberspächer, J., Golovleva, L. A., and Lingens, F. (1995) *J. Bacteriol.* **177,** 229–234
25. Daubaras, D. L., Saido, K., and Chakrabarty, A. M. (1996) *Appl. Environ. Microbiol.* **62,** 4276–4279
26. Kozyreva, L. P., Shurukhin, I., Finkelshtein, Z. I., Baskunov, B., and Golovleva, L. A. (1993) *Microbiology* (translation of *Mikrobiologiya*) **62,** 78–85
27. Solyanikova, I. P., Protopopova, Y. Y., Travkin, V., and Golovleva, L. A. (1996) *Biochemistry* (*Moscow*) **61,** 461–466
28. Lange, S. J., and Que, L., Jr. (1998) *Curr. Opin. Chem. Biol.* **2,** 159–172
29. Pieper, D. H., Pollmann, K., Nikodem, P., Gonzalez, B., and Wray, V. (2002) *J. Bacteriol.* **184,** 1466–1470
30. Travkin, V. M., Jadan, A. P., Briganti, F., Scozzafava, A., and Golovleva, L. A. (1997) *FEBS Lett.* **407,** 69–72
31. Hatta, T., Nakano, O., Imai, N., Takizawa, N., and Kiyohara, H. (1999) *J. Biosci. Bioeng.* **87,** 267–272
32. Murakami, S., Okuno, T., Matsumura, E., Takenaka, S., Shinke, R., and Aoki, K. (1999) *Biosci. Biotechnol. Biochem.* **63,** 859–865
33. Briganti, F., Mangani, S., Pedocchi, L., Scozzafava, A., Golovleva, L. A., Jadan, A. P., and Solyanikova, I. P. (1998) *FEBS Lett.* **433,** 58–62
34. Ohlendorf, D. H., Lipscomb, J. D., and Weber, P. C. (1988) *Nature* **336,** 403–405
35. Elgren, T. E., Orville, A. M., Kelly, K. A., Lipscomb, J. D., Ohlendorf, D. H., and Que, L., Jr. (1997) *Biochemistry* **36,** 11504–11513
36. Ohlendorf, D. H., Orville, A. M., and Lipscomb, J. D. (1994) *J. Mol. Biol.* **244,** 586–608
37. Orville, A. M., Elango, N., Lipscomb, J. D., and Ohlendorf, D. H. (1997) *Biochemistry* **36,** 10039–10051
38. Orville, A. M., Lipscomb, J. D., and Ohlendorf, D. H. (1997) *Biochemistry* **36,** 10052–10066
39. D'Argenio, D. A., Vetting, M. W., Ohlendorf, D. H., and Ornston, L. N. (1999) *J. Bacteriol.* **181,** 6478–6487
40. Vetting, M. W., D'Argenio, D. A., Ornston, L. N., and Ohlendorf, D. H. (2000) *Biochemistry* **39,** 7943–7955
41. Vetting, M. W., and Ohlendorf, D. H. (2000) *Struct. Fold. Des.* **8,** 429–440
42. Ferraroni, M., Solyanikova, I. P., Kolomytseva, M. P., Scozzafava, A., Golovleva, L. A., and Briganti, F. (2004) *J. Biol. Chem.* **279,** 27646–27655
43. Daubaras, D. L., Hershberger, C. D., Kitano, K., and Chakrabarty, A. M. (1995) *Appl. Environ. Microbiol.* **61,** 1279–1289
44. Golovleva, L. A., Pertsova, R. N., Evtushenko, L. I., and Baskunov, B. P. (1990) *Biodegradation* **1,** 263–271
45. Eulberg, D., Golovleva, L. A., and Schlömann, M. (1997) *J. Bacteriol.* **179,** 370–381
46. Stone, K. L., LoPresti, M. B., Crawford, J. M., DeAngelis, R., and Williams, K. R. (1989) in *A Practical Guide to Protein and Peptide Purification for Microsequencing* (Matsudaira, P. T., ed) pp. 33–47, Academic Press, San Diego
47. Sambrook, J., and Russell, D. W. (2001) *Molecular Cloning: A Laboratory Manual*, 3rd Ed., Cold Spring Harbor Laboratory Press, Cold Spring Harbor, NY
48. Marchuk, D., Drumm, M., Saulino, A., and Collins, F. S. (1991) *Nucleic Acids Res.* **19,** 1154
49. Wilson, K. (2000) in *Current Protocols in Molecular Biology* (Ausubel, F. M., Brent, R., Kingston, R. E., Moore, D. D., Seidman, J. G., Struhl, K., eds) vol. 1, pp. 2.4.1–2.4.5, John Wiley & Sons, Inc., New York
50. Altschul, S. F., Madden, T. L., Schäffer, A. A., Zhang, J., Zhang, Z., Miller, W., and Lipman, D. J. (1997) *Nucleic Acids Res.* **25,** 3389–3402
51. Thompson, J. D., Gibson, T. J., Plewniak, F., Jeanmougin, F., and Higgins, D. G. (1997) *Nucleic Acids Res.* **25,** 4876–4882
52. Benvenuti, M., Briganti, F., Scozzafava, A., Golovleva, L. A., Travkin, V. M., and Mangani, S. (1999) *Acta Crystallogr. Sect. D Biol. Crystallogr.* **55,** 901–903
53. Terwilliger, T. C., and Berendzen, J. (1999) *Acta Crystallogr. Sect. D Biol. Crystallogr.* **55,** 849–861
54. Otwinowski, Z., and Minor, W. (1997) *Methods Enzymol.* **276,** 307–326
55. Collaborative Computational, P. N. (1994) *Acta Crystallogr. Sect. D Biol. Crystallogr.* **50,** 760–763
56. Terwilliger, T. C. (2001) *Acta Crystallogr. Sect. D Biol. Crystallogr.* **57,**

1755–1762
57. Perrakis, A., Morris, R., and Lamzin, V. S. (1999) *Nat. Struct. Biol.* **6,** 458–463
58. Quanta v. 98 (1997) *Quanta Simulation, Search and Analysis*, Molecular Simulation, Inc., San Diego
59. Laskowski, R. A., MacArthur, M. W., Moss, D. S., and Thornton, J. M. (1993) *J. Appl. Crystallogr.* **26,** 283–291
60. Kabsch, W., and Sander, C. (1983) *Biopolymers* **22,** 2577–2637
61. Ritchie, D. W., and Kemp, G. J. (1999) *J. Comp. Chem.* **20,** 383–395
62. McLachlan, A. D. (1982) *Acta Crystallogr. Sect. A* **38,** 871–873
63. Nielsen, J. E., Andersen, K. V., Honig, B., Hooft, R. W., Klebe, G., Vriend, G., and Wade, R. C. (1999) *Protein Eng.* **12,** 657–662
64. Bashford, D. (1997) *ISCOPE97* **1343,** 233–240
65. DeLano, W. L. (2002) *The PyMOL Molecular Graphics System* v. 0.97, DeLano Scientific, San Carlos, CA
66. Huang, C. C., Couch, G. S., Pettersen, E. F., and Ferrin, T. E. (1996) *Pac. Symp. Biocomput.* **1,** 724
67. Sanner, M. F., Olson, A. J., and Spehner, J. C. (1996) *Biopolymers* **38,** 305–320
68. Que, L., Jr., and Watanabe, Y. (2001) *Science* **292,** 651–653
69. Eley, K. L., Crowley, P. J., and Bugg, T. D. (2001) *J. Org. Chem.* **66,** 2091–2097
70. Dorn, E., and Knackmuss, H. J. (1978) *Biochem. J.* **174,** 73–84
71. Varga, J. M., and Neujahr, H. Y. (1970) *Eur. J. Biochem.* **12,** 427–434
72. Nakai, C., Nakazawa, T., and Nozaki, M. (1988) *Arch. Biochem. Biophys.* **267,** 701–713
73. Maltseva, O. V., Solyanikova, I. P., and Golovleva, L. A. (1994) *Eur. J. Biochem.* **226,** 1053–1061

Crystal Structure of the Hydroxyquinol 1,2-Dioxygenase from *Nocardioides simplex* 3E, a Key Enzyme Involved in Polychlorinated Aromatics Biodegradation

Marta Ferraroni, Jana Seifert, Vasili M. Travkin, Monika Thiel, Stefan Kaschabek, Andrea Scozzafava, Ludmila Golovleva, Michael Schlömann and Fabrizio Briganti

J. Biol. Chem. 2005, 280:21144-21154.
doi: 10.1074/jbc.M500666200 originally published online March 16, 2005
